Molecular Modeling Studies on G-Quadruplex Complexes of Telomerase Inhibitors: Structure−Activity Relationships

Martin A. Read,[†,‡] Alexis A. Wood,[†,‡] John R. Harrison,[‡] Sharon M. Gowan,[§] Lloyd R. Kelland,[§] Harvinder S. Dosanjh,[‡] and Stephen Neidle*[,‡]

CRC Biomolecular Structure Unit, Chester Beatty Laboratories, The Institute of Cancer Research, Fulham Road, London SW3 6JB, U.K. and CRC Centre for Cancer Therapeutics, The Institute of Cancer Research, 15 Cotswold Road, Sutton, Surrey SM2 5NG, U.K.

Received June 8, 1999

Inhibition of the ability of the enzyme telomerase to add telomeric repeats to the end of chromosomes is a novel target for potential anticancer therapy. This paper examines the hypothesis that compounds possessing a planar aromatic chromophore inhibit telomerase via stabilization of, and binding to, a folded guanine quadruplex structure. Two series of telomerase inhibitors have been designed based on the 2,6-disubstituted amidoanthracene-9,10-dione and 3,6-disubstituted acridine chromophores in order to investigate structure−activity relationships between biological activity and substituent group size. The relative binding energies between these compounds and the folded human telomere DNA quadruplex were determined using molecular simulation methods, involving explicitly solvated structures. The results obtained are in excellent agreement with the biological activity as measured in vitro using a modified TRAP assay and in general agreement with the ranking order of binding enthalpies found in isothermal titration calorimetry studies. This broad agreement provides strong support for the hypothesis that guanine quadruplexes are the primary target for telomerase inhibitors with extended planar chromophores.

Introduction

Telomeres are the noncoding regions of DNA at the ends of chromosomes.[1,2] Their function is to counterbalance the truncation of the chromosome ends that occurs with each replication cycle[3] and thus prevent aberrant recombination and degradation by exonucleases. Telomeres are composed of tandem repeats of short G-rich sequences, exemplified by the human telomeric sequence 5′-TTAGGG. The ability of human germ cells, immortalized cell lines, and tumor cells to replicate indefinitely is due, at least in part, to the enzyme telomerase, a specialized ribonucleoprotein with reverse transcriptase activity and an intrinsic RNA template on which further telomeric DNA repeats are synthesized on to chromosome ends. Telomerase activity has been detected in 85−90% of all human cancers: there is increasing evidence for telomerase to have a pivotal role in proliferation, tumorigenesis, and cellular immortalization.[4−6] It is therefore a potentially highly selective target for chemotherapeutic intervention.[7] It has been shown that antisense or PNA molecules directed against the telomerase RNA template can have a high degree of potency.[8]

Guanine-rich DNA sequences have the ability to form four stranded inter- and intramolecular guanine quadruplex structures[9−12] under conditions of high sodium or potassium ionic strength. Since the RNA template of telomerase requires a nonfolded telomeric DNA primer in order to effect telomere synthesis, the formation of a telomeric G-quartet structure at high potassium ion levels results in the inhibition of telomerase function.[10,11] A number of small molecules have been discovered to inhibit the function of telomerase, by acting in an analogous way as potassium ions, to stabilize G-quadruplex structures,[13] which then effectively become trapped and cannot then function as primers for telomerase. Inhibitors based on the disubstituted tricyclic amidoanthracene-9,10-dione (AQ) chromophore were initially synthesized in this laboratory.[14] Planar aromatic chromophores are also key structural features in the inhibitors tetra-[*N*-methylpyridyl]porphyrin[15] and *N*,*N*′-bis[2-1(-piperidino)-ethyl]-3,4,9,10-perylene-tetracarboxylic diimide,[16] both of which also bind to G-quadruplexes. Several ligand−G-quadruplex complexes have been characterized, by spectroscopic and NMR studies.[15a,16] These have shown that discrete complexes are formed with the folded G-quadruplex structure[17] formed by the human telomere repeat d[$TAG_3(TTAG_3)_3$] and that a principal binding site is likely to be at the 5′-AG step.

Examination of five series of AQ regioisomers concluded that while the positional placement of the substituent aminoalkylamido side chains dictates the exact mode of binding to G-quadruplexes, it did not necessarily affect their ability to inhibit telomerase.[14c] To improve activity against telomerase, qualitative molecular modeling has been employed to identify other suitable chromophores, such as substituted fluorenones.[18] These studies also suggested that the acridine moiety, substituted in a manner analogous to the 2,7-amidoanthracene-9,10-diones, would have at least comparable G-quadruplex binding affinity, and hence telomerase activity, combined with superior physicochemical properties such as aqueous solubility. The chemistry and biological properties of these compounds will be reported elsewhere.[19]

* Correspondence to Professor S. Neidle, CRC Biomolecular Structure Unit, Chester Beatty Laboratories, The Institute of Cancer Research, Fulham Road, London SW3 6JB, U.K. Tel: 44 171 352 8133 ext 5441. E-mail: s.neidle@icr.ac.uk.

† These authors have contributed equally to this work.

‡ CRC Biomolecular Structure Unit.

§ CRC Centre for Cancer Therapeutics.

10.1021/jm990287e CCC: $18.00
Published on Web 10/15/1999

Chart 1. End-Group Substitutions (R) on the Amidoalkyl Groups Attached to the Anthracene-9,10-dione (AQ) and Acridine (AC) Chromophores

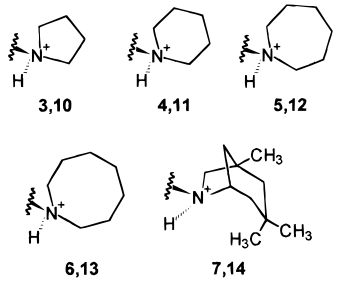

To further improve the rational design of these and other telomerase inhibitors we present here a detailed molecular modeling investigation into the effects on binding of both 2,6-disubstituted amidoanthracene-9,-10-diones (AQ) and 3,6-disubstituted acridine (AC) chromophores to the human G-quadruplex structure.[17] Systematic variations in the size of the substituent end groups on AQ and AC molecules have been examined. Earlier studies on AQ compounds have demonstrated the requirement of a cationic nitrogen atom at the terminus of each end group, as part of cyclic pyrrolidino and piperidino groups, in order for telomerase activity to be achieved in the low micromolar range.[14] Accordingly we have used cyclic ring systems with progressive increases in ring size (Chart 1).

The predictions and conclusions of the modeling are compared here with their telomerase inhibitory activity as measured in a modified TRAP assay.[14b,c] Since our approach to the design of telomerase inhibitors is based on the hypothesis of G-quadruplex stabilization, the present study provides a searching test for the hypothesis. The lack of a correlation between predicted G-quadruplex affinity and telomerase activity would indicate that the hypothesis is not a realistic one. Conversely, the establishment of a correlation can be taken as strong evidence in its favor and indicates that further rational ligand design can with confidence be based on it.

Molecular Modeling

We have adopted an approach to the calculation of intermolecular energies which is as realistic as possible, does not require the computational resources needed for formal free energy computations, and importantly enables a diversity of ligand substitutions to be examined. Simulations were performed in fully solvated and ionic environments. Relative binding energies for all compounds in the AQ and AC series were calculated by subtracting the total interaction energy of the explicitly solvated drug and its surroundings in a neutral periodic box from the identical system, when the drug was bound to the folded human G-quadruplex DNA structure. The resulting differences in interaction energy correspond to the relative binding energy. This method is adapted from a semiempirical method for calculating free energy of binding first presented by Åqvist and co-workers.[20] Although these energies are not identical to absolute thermodynamic binding energies measured by biophysical methods, we show here that this approach to the problem of predicting relative binding interaction energies for new analogues provides realistic intermolecular binding energies which do correlate with biochemical measurements of telomerase inhibition. They also are in accord with the ranking order of binding enthalpies determined by isothermal titration calorimetry and reported below. We have previously shown[14c] with equilibrium binding studies that anthraquinone ligands can form stable 1:1 complexes with the folded human G-quadruplex. We have developed[14c] a molecular model for 1:1 ligand binding to a pseudo-intercalation site at the 5′-AG step in the folded G-quadruplex structure, extrapolating from NMR studies on linear quadruplexes.[15] This forms the basis for the present modeling studies.

Scheme 1[a]

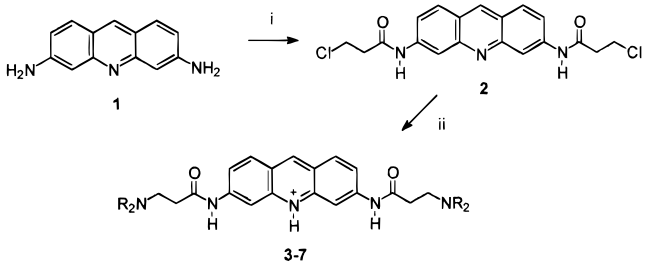

[a] Reagents and conditions: (i) chloropropionyl chloride, reflux, 2−3 h; (ii) (a) R_2N, EtOH, NaI, reflux, 3−4 h, (b) HCl.

Scheme 2[a]

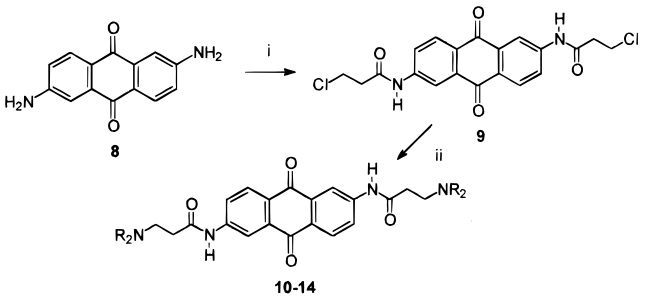

[a] Reagents and conditions: (i) chloropropionyl chloride, reflux, 2−3 h; (ii) (a) R_2N, EtOH, NaI, reflux, 3−4 h, (b) maleic acid.

Chemistry

Synthesis of the difunctionalized derivatives **3**−**7** and **10**−**14** was accomplished using procedures previously described[14,18,19] (Schemes 1 and 2). Briefly, acylation of the diamine compounds **1** and **8** with 3-chloropropionyl chloride then subsequent aminolysis by reflux treatment with the appropriate amine, in the presence of NaI catalyst, gave the desired analogues. Compounds were obtained in good yield and were adjudged pure by elemental analysis, mass spectrometry, and ^{1}H NMR. The free-base compounds were only sparingly soluble in water, hence they were converted into biologically acceptable acid addition salts in order to improve their aqueous solubility.

Results and Discussion

The 10 inhibitors used in this study are shown in Chart 1, with five in each AQ and AC series. Each successive compound in the two series has progressive increases in steric bulk by adding an additional carbon to the substituent group ring. The final compound in each series incorporates the 1,3,3-trimethyl-6-azabicyclo-[3.2.1]octano bicyclic system in order to evaluate the

Table 1. Calculated Energies (kcal/mol) for Anthraquinone (AQ) and Acridine (AC) G-Quadruplex Complexes, Together with IC_{50} Values for Telomerase Inhibition (μM), from TRAP Assay Studies

	DNA + drug in water box VdW	DNA + drug in water box electrostatic	DNA + drug in water box total energy	drug in water box only VdW	drug in water box only electrostatics	drug in water box only total energy	calculated relative binding energy	IC_{50}
				AQ G-Quadruplex Complexes				
10	−89.3	−211.6	−300.9	−58.2	−201.1	−259.2	−41.7	1.8
11	−83.9	−221.5	−305.4	−83.3	−188.8	−272.1	−33.3	4.5
12	−104.2	−200.8	−305	−80.3	−194.2	−274.5	−30.5	13
13	−103.2	−196.5	−299.7	−90.1	−188.7	−278.8	−20.9	≫50
14	−113.2	−209.5	−322.7	−98.1	−201	−299.1	−23.57	≫50
				AC G-Quadruplex Complexes				
3	−78.6	−419.7	−498.3	−66.5	−378	−444.5	−53.8	5.2
4	−83.3	−432.3	−515.6	−87.2	−359.8	−447	−68.6	2.8
5	−92.4	−372.3	−464.7	−83.4	−333.6	−417	−47.7	3.1
6	−79.3	−344.8	−424.1	−86.4	−385.1	−471.5	47.4	≫50
7	−111.3	−296.5	−407.8	−90	−426.7	−516.7	108.9	≫50

Table 2. Association Constants (K), Number of Molecules Bound per G-Quadruplex, and Binding Enthalpies ($\Delta H°$), from Isothermal Titration Calorimetry Measurements on Acridine Complexes[a]

	N	K ($\times 10^4$ M^{-1})	$\Delta H°$
3	1.05(04)	9.72(82)	−60.8(32)
4	1.10(28)	1.38(26)	−20.9(62)
5	1.19(08)	1.38(17)	−17.6(17)
6	1.03(22)	0.48(64)	−6.9(17)

[a] The folded human telomere sequence d[$AG_3(T_2AG_3)_3$] was used, and determinations were performed at 25 °C. No correction was applied for potential contributions from heats of dissociation of ligand dimers, which we have previously estimated[14c] to contribute no more than 5−10%.

effect of a large hydrophobic bulk while leaving the cationic nitrogen relatively free to interact with the G-quadruplex structure. Calculated relative binding energies for the AQ and AC series are given in Table 1, with the IC_{50} results of each compound for in vitro telomerase inhibition. The clear overall trend in both series is for the relative binding energy to increase as the steric bulk of the substituent group is increased, in excellent qualitative agreement with the telomerase inhibition data. For each series, there is a large change in binding energy as the transition is made from seven- to eight-membered rings; the larger-ring compounds are all inactive as telomerase inhibitors. Table 2 gives the binding data for four out of five members of the acridine series (the relative insolubility of the 1,3,3-trimethyl-6-azabicyclo[3.2.1]octano derivative precluded a study of its binding by isothermal titration calorimetry). Calorimetric data for compound **3** are shown in Figure 1; that for the three other compounds examined is closely comparable. These data (i) concur with the assumption of the complexes having 1:1 stoichiometry and (ii) show that the ranking order of binding enthalpies, though not their absolute values, is in overall qualitative agreement with the calculated binding energies in Table 1.

The simulations with the AQ series have predicted that the compound with highest affinity to the human G-quadruplex structure would be the one with pyrrolidine end groups (**10**). This is reflected in its low telomerase IC_{50} value, the lowest for the series. Telomerase activity decreases marginally for the six- and seven-membered ring analogues (**11** and **12**) and is effectively abolished for the larger eight-membered ring (**13**) and bicyclic (**14**) derivatives. These trends are accurately predicted by the relative binding energies calculated from the simulations. Examination of the final structures and the dynamic trajectories for all the AQ simulations reveals that the AQ chromophore position is not rigidly defined, but is free to move around in the binding site (Figure 2D,F). This allows the chromophore to compensate in part for any excessive steric interactions as a result of larger end groups.

The predicted relative binding energies for the acridine-based compounds again accurately reflect the trends in the biological data. An initial study conducted with the AFFINITY program, an automated docking module[21] in the InsightII suite, predicted the AC compounds to be stronger binding ligands to G-quadruplex DNA than the corresponding AQ ones, ostensibly due the protonated central nitrogen atom in the AC chromophore. However, although the AC series generally exhibit slightly superior telomerase activity, it is not to the degree which we initially anticipated. Examination of the simulation trajectories and final structures suggests that differences in chromophore position are significant factors in ensuring that the additional charge in the AC series does not dominate, so that overall binding of the AQ and AC series is actually broadly equivalent. The cationic center incorporated into the aromatic moiety of the AC series confines the chromophore to a specific position that limits the size of the end groups that can be accommodated. It is evident from all the AC simulations that the protonated nitrogen atom is located over the center of the adjacent G-quartet (Figure 2E). The orientation of the oxygens on each of the four guanines in the quartet are such that an area of partial negative charge is formed, strongly attracting partial cationic charges and formally protonated species. This explains why cations such as K^+ and Na^+ have been found to stabilize G-quartets via their coordination to the guanyl oxygens and represent a crucial component of the G-quadruplex system. In contrast, the AQ chromophore has a more uniform distribution of electron deficiency, with partial positive atomic charges not being localized at any one region. This is reflected in the mobility of the AQ chromophore in the intercalation site; a clear distinction can be seen when comparing the chromophore trajectories in both series (data not shown). The additional mobility of the AQ derivatives allows their protonated side chains to fully maximize electrostatic interactions with the negatively charged phosphate backbones of the G-quadruplex.

There is an abrupt change in both predicted relative binding energy and telomerase activity between compounds with seven- compared to eight-membered end

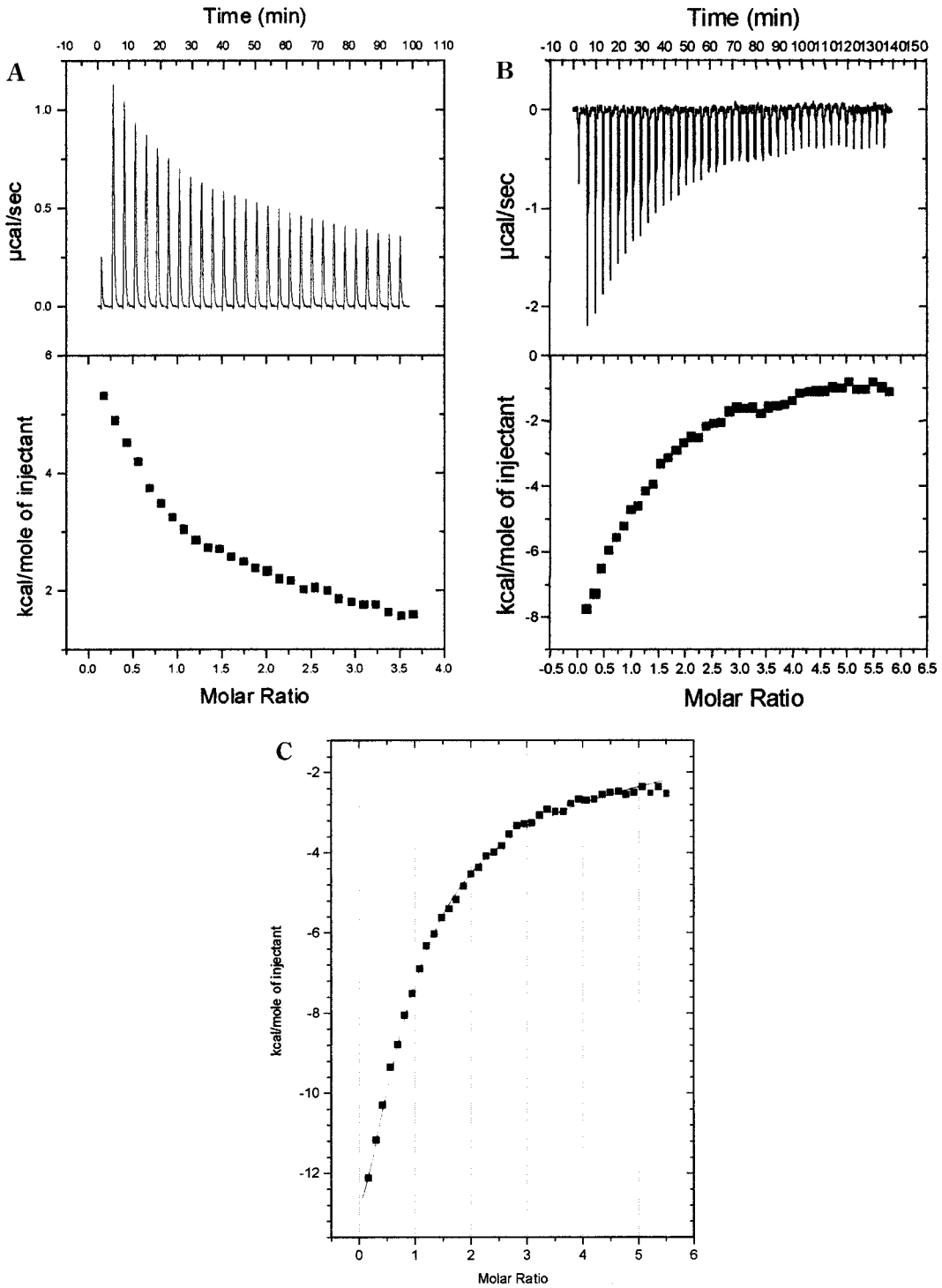

Figure 1. Calorimetric data for the titration of compound **3** with the quadruplex sequence d[$AG_3(T_2AG_3)_3$], determined at 25.00 ± 0.01 °C. Part A shows the time course for titration of drug into buffer. The peaks in the upper panels of A and B represent the power output associated with each injection of ligand as a function of time. Integration of these peaks gives the corresponding binding isotherm in the lower panels. Part B shows the titration of drug into DNA, for ligand:DNA ratios between 0 and 6.5:1. Part C shows the final binding isotherm, obtained by subtraction of the time course in part A from that in part B.

group rings. This is especially so for the AC series, where molecule **6** causes significant disruption to the G-quadruplex structure, resulting in a net positive binding energy. These positive values reflect the very considerable loss of interactions between the drug and DNA when the complex distorts. One possible explanation for this comes from a consideration of the conformational features of the seven- and eight-membered rings. The interaction of the protonated nitrogen with the negative phosphates is an important component in the ability of these compounds to bind to DNA. Increasing the steric bulk around the nitrogen not only shields it from participating in effective electrostatic interactions but also sterically restricts the formation of the anchoring hydrogen bonds. Specifically the five-, six-, and seven-membered rings are each relatively fixed in one conformation. For example, the lowest energy conformation for the six-membered ring is very dis-

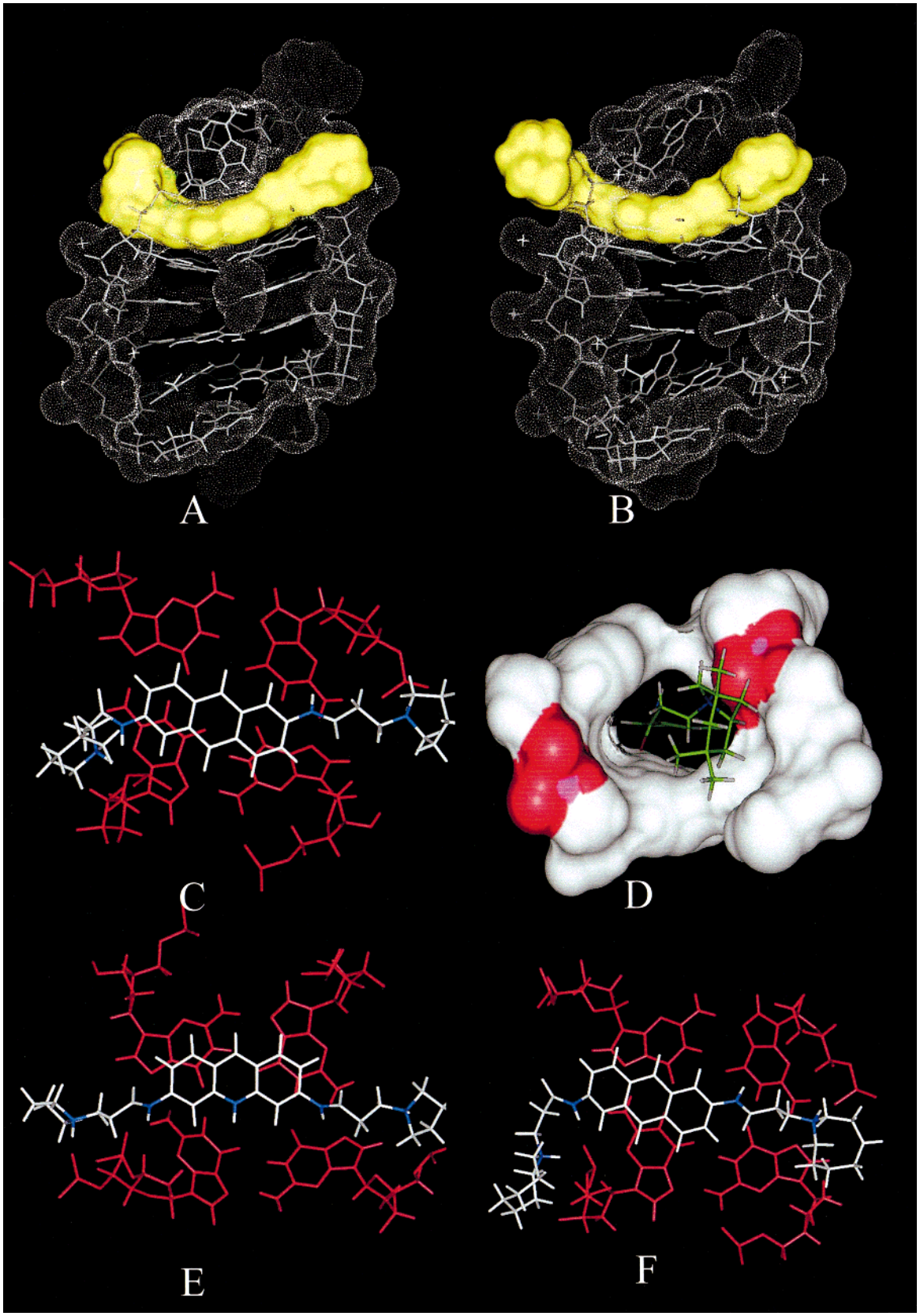

Figure 2. (A) View of a molecule of compound **11** (showing its solvent-accessible surface) and the adjacent guanine quartet (showing its dot surface). Note that the chromophore is centrally located. (B) A similar view of a molecule of **13** showing the relative mobility of the AQ chromophore. (C) A view of a molecule of compound **11**, projected onto the plane of the adjacent guanine quartet. (D) A side view of the human telomere quadruplex structure with the molecule of compound **14** bound. (E) A view of a molecule of **3**, projected onto the plane of the adjacent guanine quartet. Compound **3** possesses a central protonated nitrogen (shown dark blue) which restricts the freedom of movement of the ligand through its interaction with the guanyl oxygen atoms. (F) A view of a bound molecule of **13**, showing it shifted to one side of the binding site.

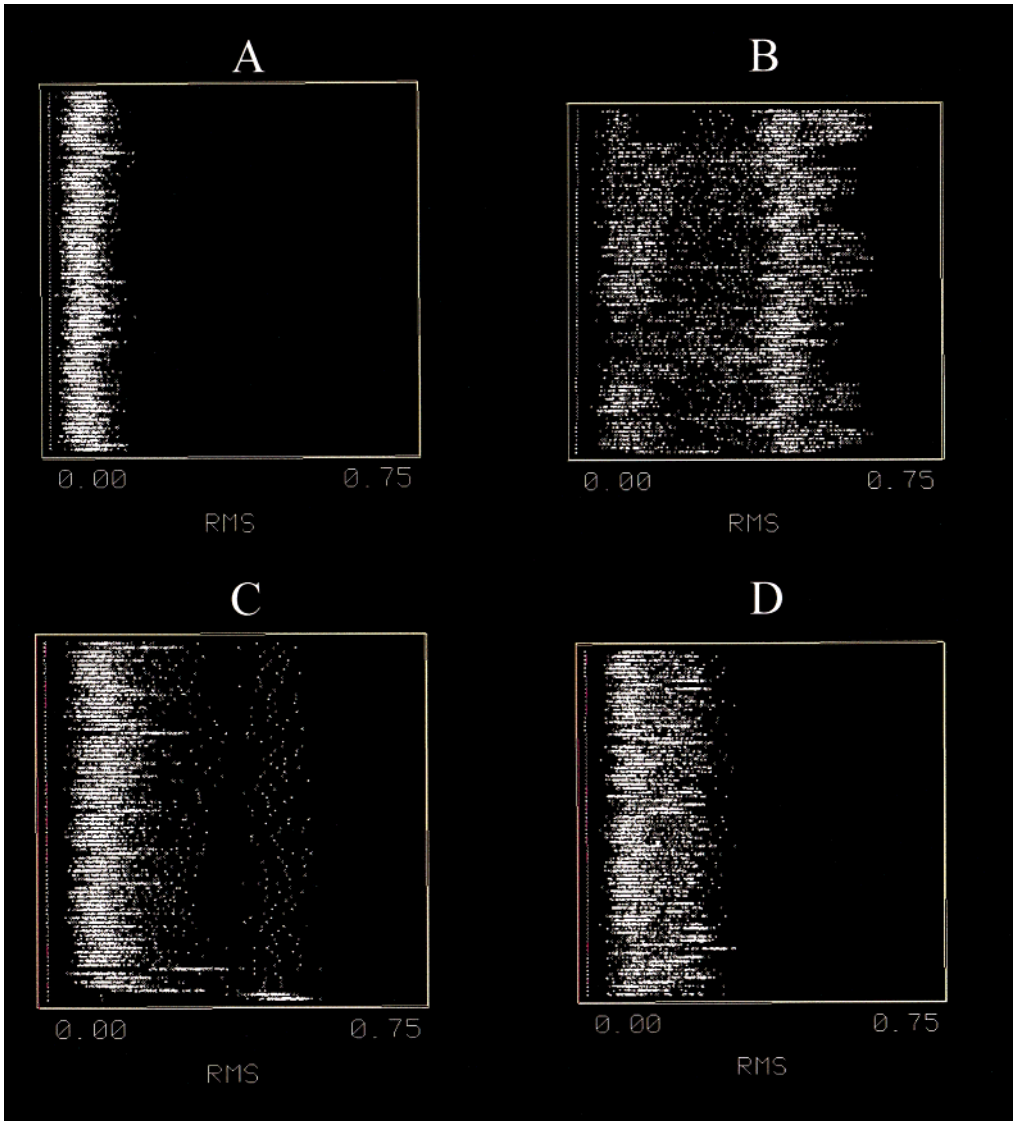

Figure 3. Cluster plots of the RMS deviations in atomic positions for the cyclic carbon atoms alone of the anthracene-9,10-dione derivatives, following the superposition of every snapshot from each molecular dynamics simulation of a quadruplex complex: (A) for **11**, (B) for **12**, (C) for **13**, (D) for **14**. In each case the *y*-axis represents snapshot number, going from 1 to 80.

tinctly of chair-type, with the largest substituents in the equatorial positions. A significant energy barrier must be overcome in order to flip to the boat conformation, especially when there are large substituents.

Figure 3 shows the RMS cluster plots for the side chain ring moieties in the AQ series, with each snapshot throughout the trajectory being compared to all the others (only the ring carbon atoms are included). The resulting plot reveals the scale of the conformational differences seen throughout the simulation, where large changes in ring conformation produce a spreading of cluster points into the region of high RMS values. Unsurprisingly, the rigidity of the five- and six-membered rings is reflected in their virtually identical cluster plots, (only that for compound **11** is shown; Figure 3A), where the majority of the cluster points are very close at low RMS values. There are two noticeable families of conformations for the seven-membered ring, one comprising chair and twist-chair, the other boat and twist-boat conformers. The situation is quite similar to that for the six-membered ring compound, except that in this case the chair is part of a family of flexible conformations, with the twist-chair being slightly more stable due to eclipsing at the flat end. The cluster plot (Figure 3B) reflects this pseudo-rotation as the cluster points are far more spread out and reach into the region of larger RMS values. The eight-membered ring has the freedom to pseudo-rotate between the conformations in each family, although the boat-chair family is significantly more stable than the other families.[22] This feature is readily observed in the trajectories of this compound and results in a cluster plot (Figure 3C), where the majority of the conformations remain in the boat-chair family, with some pseudo-rotating into other families during the trajectory. Consequently, the mobility of the eight-membered ring is enhanced, and the end group struggles to maintain the hydrogen bonds to the backbone, reducing its effective binding.

The bicyclic 1,3,3-trimethyl-6-azabicyclo[3.2.1]octano derivatives, on the other hand, still remain rigidly restrained and disrupt the quadruplex structure by expanding the grooves solely on account of their size—see the low region of RMS values in the cluster plot for the bicyclic compound (Figure 3D). The expansion of groove widths has been monitored by measuring the distance between the backbone phosphate groups on

adjacent strands, at the pseudo-intercalation site of ligand binding. A clear trend is apparent, with groove width increasing steadily with substituent group steric bulk. P···P distances are 11.5, 12.4, and 13.5 Å for the five-, six-, and seven-membered ring compounds, respectively. For the eight-membered ring compounds **6** and **13**, the ligand is shifted out of the intercalation site (Figure 2F), and the groove widths reduce to 10.9 Å, a clear indication that the eight-membered ring cannot be readily accommodated in the grooves. This is particularly noticeable in Figure 2B, where the side chain protrudes out of the DNA groove to a much greater extent than, for example, the corresponding pyrrolidine analogue (Figure 2A). The bicyclic analogues **7** and **14** produce an increase in groove width of approximately 2−3 Å compared to the pyrrolidine compounds. This results in a severe distortion of the ligand−G-quadruplex complex, although the side chains of the ligands still maintain relatively stable electrostatic interactions with the backbone phosphate groups (Figure 2D).

We conclude that this molecular modeling study has been successful in correctly predicting (i) the relative G-quadruplex binding abilities and (ii) telomerase inhibitory activities of two series of planar aromatic telomerase inhibitors. This provides strong correlative support for the hypothesis that the mode of action of these molecules is via interaction with four-stranded G-quadruplex DNA structures[14a,15,23] and provides a firm foundation for further structure-based rational design of ligands with enhanced selectivity and activity.

Experimental Section

Molecular Modeling. The InsightII suite of programs and the CFF force field developed and validated by Molecular Simulations Inc. was used for all model building and calculations.[24] The coordinates for the solution NMR structure[17] of the folded intramolecular G-quadruplex human telomeric repeat d[$TAG_3(TTAGGG)_3$] (Protein Data Bank entry 143D) were used as an initial starting model. This system was initially subjected to molecular mechanics energy minimization (1000 steps steepest descent and 3 × 1000 steps Polak-Ribiere conjugate gradient), followed by 140 ps of molecular dynamics simulation (1.5 fs time step, at 300 K). The subsequent time-averaged structure was further minimized (1000 steps steepest descent and 3 × 1000 steps Polak Ribiere conjugate gradient) and used as the basis for all further modeling studies.

A pseudo-intercalation site was introduced between the diagonal T_2A loop and the G-quartet segment of the structure (at the 5′-AG step) by breaking the two phosphate backbones and separating the two halves of the structure so that the separation of the A·G base pair and G-quartet increased from 3.4 to 6.8 Å. The sugar−phosphate chains were reconnected, and molecular mechanics energy minimization (1000 steps steepest descent with line searching followed by 1000 steps conjugate gradient) was used to relieve any resulting steric distortion while retaining the intercalation geometry between G-quartet and loop motifs by means of appropriate positional restraints.

Molecular models of the five derivatives in each AQ and AC series were built and energy minimized using the same computational steps as described for the G-quadruplex. The minimized ligands were, in turn, docked into the intercalation site. Initially, several possible orientations of the drugs in the intercalation site were evaluated using manual docking within the AFFINITY[21] module of the InsightII package. This method enables the rapid estimation of potentially low energy positions to be made while simultaneously monitoring electrostatic and van der Waals contributions to the total interaction energy. Fixed docking was then employed to examine the most favorable orientations more thoroughly using a Monte Carlo procedure while allowing the drug atoms and defined binding-site atoms to move. If the resulting ligand/receptor system was within the predefined energy tolerance of the previous structure, the system was subjected to minimization. The resulting structure was accepted based upon an energy check, which uses Metropolis criterion, and also a check of the RMS distance of the new structure versus structures found so far. The final conformations of each drug−DNA complex were then obtained through a further round of 100 steps of minimization where the resulting interaction energy values were used to define a ranking order.

The highest ranked structure in each case was placed in a 45 Å cubic cell. A sodium counterion was positioned between each pair of guanine quartet planes, as described in the crystal structure of the d(TG_4T) quadruplex.[25] An additional 22 sodium counterions were included to neutralize the charge of the DNA backbone. Chlorine ions were included at random positions within the cell to neutralize the charge on the inhibitor (two anions for the anthracene-9,10-dione structures, three anions for the acridine structures) and a further two chlorine ions were added to balance the sodium cations between the guanine quartets. The cell was then solvated with explicit preequilibrated water molecules.

The equilibration protocol comprised 1000 steps of steepest descent/conjugate gradient minimization, followed by a 20 ps simulation while constraining the DNA, inhibitor, and ions. The constraints were removed and a further 300 steps of minimization were performed, followed by a 30 ps simulation during which the DNA, inhibitor, and ions were restrained. These restraints were gradually relaxed during this simulation. The final production simulation was 110 ps in duration, and restraints were placed on the guanine amino groups to ensure their coplanarity with the ring system.

The telomeric DNA and its associated backbone counterions were deleted from the initial structure before solvating the 45 Å cubic cell. The resulting neutral system was equilibrated in an identical manner to the inhibitor/DNA complex. After analyzing the trajectories for one free inhibitor, it was found that a production run of 50 ps was of sufficient duration to obtain a stable interaction energy with the solvent.

The time-averaged structures from the resulting trajectories were minimized (3000 steps) to yield the final structure to be used for interaction energy measurements. This was accomplished using the DOCKING module available as part of the Insight II molecular modeling package. Direct calculations of the contributions of the van der Waals and electrostatic components of the total interaction energy between each ligand and its environment were made for both the bound and unbound states.

Isothermal Titration Calorimetry. Calorimetric experiments on compounds **3**−**7** were carried out using the isothermal titration module of a Microcal MCS high-sensitivity titration calorimeter (Microcal Inc., Northampton, MA). Data acquisition and analysis were performed using the Origin 4.10 software package (supplied by the manufacturer). All experiments were conducted at 25.00 ± 0.01 °C in aqueous buffer (10 mM Tris HCl, 150 mM KCl, pH 7.0). The human telomeric DNA sequence d[$AG_3(T_2AG_3)_3$] was purchased from Oswel Ltd. (Southampton, U.K.) and was used without further purification. Nondenaturing polyacrylamide gels were used to show that a single folded species was formed in the presence of the KCl and that this was indistinguishable from that formed in the presence of NaCl. Binding isotherms were determined by serial 5 μL injections of ligand solution (1.4 mM) at 400 s intervals from a 250 μL syringe rotating at 400 rpm into DNA solution (37 μM). The raw calorimetric data were integrated and corrected for sample concentration and cell volume affording the heat output per injection. Control experiments were performed to determine the heats of dilution for ligand titrated into buffer, and the binding isotherm for each ligand−DNA interaction was calculated by subtraction of the heat of dilution.[14c] The binding enthalpy ($\Delta H°$), equilibrium binding constant (K_b), and stoichiometry (n) for each ligand−DNA

interaction were determined from the corrected binding isotherms using a nonlinear least-squares fitting procedure. It was not possible to obtain reliable data on several compounds in the AQ series, due to solubility problems, so only data on the AC series is reported here.

Synthetic Chemistry. Melting points (mp) were recorded on a Leica Galen III hot-stage melting point apparatus and are uncorrected. NMR spectra were recorded at 250 MHz on a Bruker AC25O spectrometer in either Me_2SO-d_6 or $CDCl_3$ solution at 303 ± 1 K using Me_4Si as internal standard. EI (70 eV), FAB, and accurate mass spectra were determined by The School of Pharmacy (University of London, U.K.). Elemental analyses were carried out by Medac Ltd. (Brunel Science Center, Egham, Surrey, U.K.); results for elements indicated by symbols were within ±0.4% of theoretical values. TLC was carried out on silica gel (Merck 60F-254) using $CHCl_3$−MeOH as eluent, with visualization at 254 and 366 nm. 3-Chloropropionyl chloride was freshly distilled before use. Organic solutions were dried over sodium sulfate.

2,6-Bis(3-chloropropionamido)anthracene-9,10-dione (**9**) was prepared as previously described.[14b,c,d] The synthesis of compound **11** has also been previously reported by us.[14d]

2,6-Bis(3-chloropropionamido)acridine (2). A solution of proflavine (5 g, 23.9 mmol) in 3-chloropropionyl chloride (20 mL) was refluxed for 2 h, cooled to 0 °C, filtered, and washed with EtOH (2 × 30 mL) and ether (2 × 20 mL). Recrystalization from DMF−EtOH (5:1 v/v) gave the propionamide **2** (7.87 g, 92%) as dark yellow crystals: NMR (DMSO) δ 3.06 (4H, t, J = 5.9 Hz, $COCH_2CH_2Cl$), 3.96 (4H, t, J = 5.9 Hz, $COCH_2CH_2Cl$), 7.85 (2H, d, J = 9.1 Hz, H-2,7), 8.36 (2H, d, J = 9.1 Hz, H-1,8), 8.89 (2H, s, H-4,5), 9.59 (1H, s, H-9), 11.42 (2H, s br, CONH).

3,6-Bis(3-piperidinopropionamido)acridine (4). To a stirred refluxing suspension of 3,6-bis(3-chloropropionamido)-acridine (1.50 g, 3.8 mmol) and NaI (0.3 g) in EtOH (50 mL) was added dropwise piperidine (2.5 mL, 30 mmol) in EtOH (10 mL). The mixture was stirred at reflux for 3 h, cooled to 0 °C, filtered, and washed with ether (50 mL). Recrystallization from DMF−EtOH (4:1 v/v) gave **4** (1.53 g, 82%) as a pale yellow solid: mp 249−250 °C; NMR ($CHCl_3$) δ 1.61 (4H, m, $N(CH_2CH_2)_2CH_2$), 1.77 (8H, m, $N(CH_2CH_2)_2CH_2$) 2.59 (4H, t, J = 6.3 Hz, $COCH_2CH_2N$), 2.61 (8H, m, $N(CH_2CH_2)_2CH_2$), 2.72 (4H, t, J = 6.3 Hz, $COCH_2CH_2N$), 7.92 (4H, m, H-1,2,7,8), 8.16 (2H, m, H-4,5), 8.60 (1H, s, H-9), 11.79 (2H, s br, CONH); MS (rel intensity) m/z 488 (100), calcd ($[M + H]^+$) 488.3026, found 488.3040. Anal. ($C_{29}H_{38}N_5O_2$) C, H, N. Trihydrochloride salt mp 256−258 °C.

3,6-Bis(3-pyrrolidinopropionamido)acridine (3). The general procedure using pyrrolidine gave **3** (1.37 g, 78%) as a pale yellow solid: mp 251−252 °C; NMR (DMSO) δ 1.95 (8H, m, $N(CH_2CH_2)_2$), 2.61 (4H, t, J = 6.2 Hz, $COCH_2CH_2N$), 2.73 (8H, m, $N(CH_2CH_2)_2$), 2.90 (4H, t, J = 6.2 Hz, $COCH_2CH_2N$), 7.9 (6H, m, H-1,2,4,5,7,8), 8.58 (1H, s, H-9), 11.68 (2H, s br, CONH); MS (rel intensity) m/z 460 (100), calcd ($[M + H]^+$) 460.2713, found 460.2700. Anal. ($C_{27}H_{34}N_5O_2$) C, H, N. Trihydrochloride salt mp 266−267 °C.

3,6-Bis[3-(hexamethyleneimino)pipiperizinopropionamido]acridine (5). The general procedure with hexamethyleneimine gave **5** (1.57 g, 79%) as pale yellow crystals: mp 245−246 °C; NMR ($CDCl_3$) δ 1.80 (16H, m, CH_2), 2.54 (4H, m, $COCH_2NH_2N$), 2.82 (12H, m, NCH_2), 7.92 (4H, m, H-1,2,7,8), 8.16 (2H, m , H-4,5), 8.60 (1H, s, H-9), 11.79 (2H, s br, CONH); MS (rel intensity) m/z 516 (100), calcd ($[M + H]^+$) 516.3399, found 516.3381. Anal. ($C_{31}H_{41}N_5O_2$) C, H, N. Trihydrochloride salt mp 246−248 °C.

3,6-Bis[3-(heptamethyleneimino)pipiperizinopropionamido]acridine (6). The general procedure with heptamethyleneimine gave **6** (1.32 g, 66%) as yellow crystals: mp 241−242 °C; NMR ($CDCl_3$) δ 1.49 (20H, m, CH_2), 2.51 (12H, m, NCH_2), 2.81 (4H, t, J = 6.5 Hz, $COCH_2CH_2N$), 7.92 (4H, m, H-1,2,7,8), 8.16 (2H, m, H-4,5), 8.60 (1H, s, H-9), 11.79 (2H, s br, CONH); MS (rel intensity) m/z 248 (100), calcd ($[M + H]^+$) 544.3652, found 544.3623. Anal. ($C_{33}H_{44}N_5O_2$) C, H, N. Trihydrochloride salt mp 223−224 °C.

3,6-Bis[3-(1,3,3-trimethyl-6-azabicyclo[3.2.1]octano)-propionamido]acridine (7). The general procedure with 1,3,3-trimethyl-6-azabicyclo[3.2.1]octane gave **7** (1.80 g, 75%) as orange crystals: mp >360 °C; NMR ($CDCl_3$) δ 1.00 (6H, s, CH_3), 1.11 (6H, s, CH_3), 1.25 (4H, m, CH_2), 1.34 (6H, s, CH_3), 1.46 (4H, m, CH_2), 1.68−1.89 (4H, m, CH_2), 2.22 (2H, m, CH), 2.50 (4H, t, J = 5.3 Hz, $COCH_2$), 2.80−3.05 (4H, m, $COCH_2CH_2N$), 3.20−3.30 (4H, m, CH_2), 7.92 (4H, m, H-1,2,7,8), 8.16 (2H, m, H-4,5), 8.60 (1H, s, H-9), 11.79 (2H, s br, CONH); MS (rel intensity) m/z 624 (100), calcd ($[M + H]^+$) 624.4278, found 624.4236. Anal. ($C_{39}H_{53}N_5O_2$) C, H, N. Trihydrochloride salt mp 218−220 °C.

2,6-Bis(3-pyrrolidinopropionamido)anthracene-9,10-dione (10). The general procedure using pyrrolidine gave **10** (1.94 g, 94%) as a brown powder: mp >300 °C dec; NMR (DMSO) δ 1.68 (8H, m, $N(CH_2CH_2)_2$), 2.50 (8H, m, $N(CH_2CH_2)_2$), 2.57 (4H, t, J = 6.8 Hz, $COCH_2CH_2N$), 2.74 (4H, t, J = 6.8 Hz, $COCH_2CH_2N$), 8.05 (2H, dd, J = 8.6 and 2.0 Hz, H-3,7), 8.15 (2H, d, J = 8.6 Hz, H-4,8), 8.44 (2H, d, J = 2.0 Hz, H-1,5), and 10.70 (2H, s, D_2O removes, CONH); MS (rel intensity) m/z 488 ($[M]^{\bullet+}$, 4), 417 ($[M\text{-}C_4H_9N]^{\bullet+}$, 8), 346 ($[M\text{-}C_8H_{18}N_2]^{\bullet+}$, 34), 292 ($[M\text{-}C_{11}H_{20}N_2O]^{\bullet+}$, 20), 238 ($[M\text{-}C_{14}H_{22}N_2O_2]^{\bullet+}$, 7), 84 ($[C_5H_{10}N]^{\bullet+}$, 42), and 55 ($[C_3H_3O]^{\bullet+}$, 100). Anal. ($C_{28}H_{32}N_4O_4 \cdot 0.25H_2O$) C, H, N. Diacetate: mp >300 °C dec.

2,6-Bis[3-(hexamethyleneimino)propionamido]anthracene-9,10-dione (12). The general procedure using hexamethyleneimine gave **12** (1.28 g, 65%) as a pale yellow solid: mp >360 °C; NMR ($CDCl_3$) δ 1.80 (16H, m, CH_2), 2.54 (4H, m, $COCH_2$), 2.82 (12H, m, NCH_2), 8.06 (2H, d, J = 2.1 Hz, H-1,5), 8.26 (2H, d, J = 8.5 Hz, H-4,8), 8.34 (2H, dd, J = 8.5 and 2.1 Hz, H-3,7), 11.99 (2H, s, D_2O removes, CONH); MS (rel intensity) m/z 545 (100), calcd ($[M + H]^+$) 545.3128, found 545.3110. Anal. ($C_{32}H_{40}N_4O_4$) C, H, N. Maleate: mp 202 °C.

2,6-Bis[3-(heptamethyleneimino)propionamido]anthracene-9,10-dione (13). The general procedure using heptamethyleneimine gave **13** (1.89 g, 92%) as a yellow solid: mp 258−259 °C; NMR (DMSO) δ 1.49 (20H, m, CH_2), 2.51 (12H, m, NCH_2), 2.81 (4H, t, J = 6.5 Hz, $COCH_2$), 8.10 (2H, dd, J = 8.6 and 2.0 Hz, H-3,7), 8.16 (2H, d, J = 8.6 Hz, H-4,8), 8.42 (2H, d, J = 2.0 Hz, H-1,5), 10.56 (2H, s, D_2O removes, CONH); MS (rel intensity) m/z 573 (100), calcd ($[M + H]^+$) 573.3441, found 573.3420. Anal. ($C_{34}H_{44}N_4O_4$) C, H, N. Maleate: mp 189−190 °C.

2,6-Bis[3-(1,3,3-trimethyl-6-azabicyclo[3.2.1]octano)-propionamido]anthracene-9,10-dione (14). The general procedure using 1,3,3-trimethyl-6-azabicyclo[3.2.1]octane gave **14** (3.3 g, 70%) as a yellow solid: mp 255−256 °C; NMR ($CDCl_3$) δ 1.00 (6H, s, CH_3), 1.11 (6H, s, CH_3), 1.25 (4H, m, CH_2) 1.34 (6H, s, CH_3), 1.46 (4H, m, CH_2), 1.68−1.89 (4H, m, CH_2), 2.22 (2H, m, CH), 2.50 (4H, t, J = 5.3 Hz, $COCH_2$), 2.80−3.05 (4H, m, $COCH_2CH_2N$), 3.20−3.30 (4H, m, CH_2), 8.09 (2H, d, J = 2.1 Hz, H-1,5), 8.25 (2H, d, J = 8.5 Hz, H-4,8), 8.35 (2H, d, J = 8.5 and 2.1 Hz, H-3,7), 11.24 (2H, s, D_2O removes, CONH); MS (rel intensity) m/z 653 (100), calcd ($[M + H]^+$) 653.4067, found 653.4040. Anal. ($C_{40}H_{52}N_4O_4$) C, H, N. Maleate: mp 204 °C.

Modified Telomeric Repeat Amplification Protocol (TRAP) Assay. The ability of agents to inhibit telomerase in a cell-free assay was assessed with a modified TRAP assay using extracts from exponentially growing A2780 human ovarian carcinoma cells as described previously.[14b,c,18] The TRAP assay was performed in two steps: (a) telomerase-mediated extension of the forward primer (TS: 5′-AATCCGTCGAGCAGAGTT, Oswel Ltd., Southampton, U.K.) contained in a 40 μL reaction mix comprising TRAP buffer (20 mM Tris-HCl (pH 8.3), 68 mM KCl, 1.5 mM $MgCl_2$, 1 mM EGTA, 0.05% v/v Tween 20), 0.05 μg bovine serum albumin, 50 μM of each deoxynucleotide triphosphate, 0.1 μg TS primer, and 3 μCi of [α-^{32}P]dCTP (Amersham plc, U.K.). Protein (0.04 μg) was then incubated with the reaction mix ± agent (acid addition and quaternary dimethiodide salts) at final concentrations of up to 50 μM for 20 min at 25 °C. A lysis buffer (no protein) control, heat-inactivated protein control, and 50% protein (0.02 μg) control were included in each assay. (b) While

heating at 80 °C in a PCR block of a thermal cycler (Hybaid, U.K.) for 5 min to inactivate telomerase activity, 0.1 μg of reverse CX primer (3′-AATCCCATTCCCATTCCCATTCCC-5′) and 2 units of *Taq* DNA polymerase ("red hot", Advanced Biotechnologies) were added. A three-step PCR was then performed: 94 °C for 30 s, 50 °C for 30 s, and 72 °C for 1 min for 31 cycles. Telomerase-extended PCR products in the presence or absence of compounds were then determined either by (a) electrophoretic separation using 8% w/w acrylamide denaturing gels and analysis by phosphorimaging or autoradiography or by (b) harvesting on Whatman filters (25 mm glass microfiber) and analysis by liquid scintillation counting.

Acknowledgment. This work was supported by the Cancer Research Campaign (Program Grant SP1384 to S.N.) and by The Institute of Cancer Research (research studentship to M.A.R.). We are grateful to Heath Scientific for the use of ITC instrumentation.

References

(1) Blackburn, E. H. Structure and function of telomeres. *Nature* **1991**, *350*, 569−573.

(2) Meyne, J.; Ratliff, R. L.; Moyzis, R. K. Conservation of the human telomere sequence $(TTAGGG)_n$ among vertebrates. *Proc. Natl. Acad. Sci. U.S.A.* **1989**, *86*, 7049−7053.

(3) Harley, C. B.; Futcher, A. B.; Greider, C. W. Telomeres Shorten During Aging of Human Fibroblasts. *Nature* **1990**, *345*, 458−460. (b) Allsopp, R. C.; Harley, C. B. Evidence for a Critical Telomere Length in Senescent Human Fibroblasts. *Exp. Cell Res.* **1995**, *219*, 130−136.

(4) Kim, N. W.; Piatyszek, M. A.; Prowse, K. R.; Harley, C. B.; West, M. D.; Ho, P. L. C.; Coviello, G. M.; Wright, W. E.; Weinrich, R. L.; Shay, J. W. Specific Association of Human Telomerase Activity with Immortal Cells and Cancer. *Science* **1994**, *266*, 2011−2015. (b) Counter, C. M.; Hirte, H. W.; Bacchetti, S.; Harley, C. B. Telomerase Activity in Human Ovarian Carcinoma. *Proc. Natl. Acad. Sci. U.S.A.* **1994**, *91*, 2900−2904. (c) Tang, R.; Cheng, A.-J.; Wang, J.-Y.; Wang, T.-C. V. Close Correlation between Telomerase Expression and Adenomatous Polyp Progression in Multistep Colorectal Carcinogenesis. *Cancer Res.* **1998**, *58*, 4052−4054. (d) Hoos, A.; Hepp, H. H.; Kaul, S.; Ahlert, T.; Bastert, G.; Wallwiener, D. Telomerase Activity Correlates with Tumor Aggressiveness and Reflects Therapy Effect in Breast Cancer. *Int. J. Cancer* **1998**, *79*, 8−12. (e) Sano, T.; Asai, A.; Fujimaki, T.; Kirino, T. Telomerase Activity in 144 Brain Tumours. *Br. J. Cancer* **1998**, *77*, 1633−1637.

(5) Bodnar, A. G.; Ouellette, M.; Frolkis, M.; Holt, S. E.; Chiu, C. P.; Morin, G. B.; Harley, C. B.; Shay, J. W.; Lichtsteiner, S.; Wright, W. E. Extension of Life-span by Introduction of Telomerase into Normal Human Cells. *Science* **1998**, *279*, 349−352. (b) Niida, H.; Matsumoto, T.; Satoh, H.; Shiwa, M.; Tokutake, Y.; Furuichi, Y.; Shinkai, Y. Severe Growth Defect in Mouse Cells Lacking the Telomerase RNA Component. *Nature Genet.* **1998**, *19*, 203−206. (c) Blasco, M. A.; Lee, H.-W.; Hande, M. P.; Samper, E.; Lansdorp, P. M.; DePinho, R. A.; Greider, C. W. Telomere Shortening and Tumor Formation by Mouse Cells Lacking Telomerase RNA. *Cell* **1997**, *91*, 25−34. (d) Lee, H.-W.; Blasco, M. A.; Gottlieb, G. J.; Horner, J. W.; Greider, C. W.; DePinho, R. A. Essential Role of Mouse Telomerase in Highly Proliferative Organs. *Nature* **1998**, *392*, 569−574.

(6) Greider, C. W. Telomerase Activation. One Step on the Road to Cancer? *Trends in Genetics* **1999**, *15*, 109−112. (b) Zhu, J.; Wang, H.; Bishop, J. M.; Blackburn, E. H. Telomerase Extends the Life-span of Virus-transformed Human Cells without Net Telomere Lengthening. *Proc. Natl. Acad. Sci. U.S.A.* **1999**, *96*, 3723−3728. (c) Counter, C. M.; Hahn, W. C.; Wei, W.; Caddle, S. D.; Beijersbergen, R. L.; Lansdorp, P. M.; Sedivy, J. M.; Weinberg, R. A. Dissociation among in vitro Telomerase Activity, Telomere Maintenance and Cellular Immortalization. *Proc. Natl. Acad. Sci. U.S.A.* **1998**, *95*, 14723−14728. (d) Rudolph, K. L.; Chang, S.; Lee, H.-W.; Blasko, M.; Gottlieb, G. J.; Greider, C.; DePinho, R. A. Longevity, Stress Response and Cancer in Aging Telomerase-Deficient Mice. *Cell* **1999**, *96*, 701−712.

(7) Perry, P. J.; Kelland, L. R. Telomeres and Telomerase: Targets for Cancer Chemotherapy. *Exp. Opin. Ther. Patents* **1998**, *8*, 1567−1586. (b) Raymond, E.; Sun, D.; Chen, S.-F.; Windle, B.; von Hoff, D. D. Agents that Target Telomerase and Telomeres. *Curr. Opin. Biotech.* **1996**, *7*, 583−591. (c) Pitts, A. E.; Corey, D. R. The Telomerase Challenge − an Unusual Problem in Drug Discovery. *Drug Discovery Today* **1999**, *4*, 155−161.

(8) Hamilton, S. E.; Pitts, A. E.; Katipally, R. R.; Jia, X.; Rutter, J. P.; Davies, B. A.; Shay, J. W.; Wright, W. E.; Corey, D. R. Identification of Determinants for Inhibitor Binding within the RNA Active Site of Human Telomerase Using PNA Scanning. *Biochemistry* **1997**, *36*, 11873−11880. (b) Kondo, S.; Kondo, Y.; Li, G.; Silverman, R. H.; Cowell, J. K. Targeted Therapy of Human Malignant Glioma in a Mouse Model by 2-5A Antisense Directed Against Telomerase RNA. *Oncogene* **1998**, *16*, 3323−3330. (c) Bisoffi, M.; Chakerian, A. E.; Fore, M. L.; Bryant, J. E.; Hernandez, J. P.; Moyzis, R. K.; Griffith, J. K. Inhibition of Human Telomerase by a Retrovirus Expressing Telomeric Antisense RNA. *Eur. J. Cancer* **1998**, *34*, 1242−1249. (d) Glukhov, A. I.; Zimnik, O. V.; Gordeev, S. A.; Severin, S. E. Inhibition of Telomerase Activity of Melanoma Cells *in Vitro* by Antisense Oligonucleotides. *Biochem. Biophys. Res. Commun.* **1998**, *248*, 368−371. (e) Harrison, J. G.; Frier, C.; Laurant, R.; Dennis, R.; Raney, K. D.; Balasubramanian, S. Inhibition of human Telomerase by PNA-cationic Peptide Conjugates. *Bioorg. Med. Chem. Lett.* **1999**, *9*, 1273−1278.

(9) Williamson, J. R. G-quartet structures in telomeric DNA. *Annu. Rev. Biophys. Biomol. Struct.* **1994**, 23, 703−730.

(10) Zahler, A. M.; Williamson, J. R.; Cech, T. R.; Prescott, D. M. Inhibition of Telomerase by G-quartet DNA Structures. *Nature* **1991**, *350*, 718−720.

(11) Fletcher, T. M.; Sun, D.; Salazar, M.; Hurley, L. H. Effect of DNA Secondary Structure on Human Telomerase Activity. *Biochemistry* **1998**, *37*, 5536−5541. (b) Sun, D.; Lopez-Guajardo, C. C.; Quada, J.; Hurley, L. H.; Von Hoff, D. D. Regulation of Catalytic Activity and Processivity of Human telomerase. *Biochemistry* **1999**, *38*, 4037−4044.

(12) Marathias, V. M.; Bolton, P. H. Determinants of DNA Quadruplex Structural Type: Sequence and Potassium Binding. *Biochemistry* **1999**, *38*, 4355−4364.

(13) Mergny, J.-L.; Hélène, C. G-Quadruplex DNA: a Target for Drug Design. *Nature Med.* **1998**, *4*, 1366−1367.

(14) Sun, D.; Thompson, B.; Cathers, B. E.; Salazar, M.; Kerwin, S. M.; Trent, J. O.; Jenkins, T. C.; Neidle, S.; Hurley, L. H. Inhibition of Human Telomerase by a G-Quadruplex-Interactive Compound. *J. Med. Chem.* **1997**, *40*, 2113−2116. (b) Perry, P. J.; Gowan, S. M.; Reszka, A. P.; Polucci, P.; Jenkins, T. C.; Kelland, L. R.; Neidle, S. 1,4- and 2,6-Disubstituted Amidoanthracene-9,10-dione Derivatives as Inhibitors of Human Telomerase. *J. Med. Chem.* **1998**, *41*, 3253−3260. (c) Perry, P. J.; Reszka, A. P.; Wood, A. A.; Read, M. A.; Gowan, S. M.; Dosanjh, H. S.; Trent, J. O.; Jenkins, T. C.; Kelland, L. R.; Neidle, S. Human Telomerase Inhibition by Regioisomeric Disubstituted Amidoanthracene-9,10-diones. *J. Med. Chem.* **1998**, *41*, 4873−4884. (d) Agbandje, M.; Jenkins, T. C.; Mckenna, R.; Reszka, A. P.; Neidle, S. Anthracene-9,10-diones as Potential Anticancer Agents. Synthesis, DNA Binding and Biological Studies on a Series of 2,6-Disubstituted Derivatives. *J. Med. Chem.* **1992**, *35*, 1418−1429.

(15) Wheelhouse, R.; Sun, D.; Han, H.; Han, F. X.; Hurley, L. H. Cationic Porphyrins as Telomerase Inhibitors: the Interaction of Tetra-(*N*-methyl-4-pyridyl)porphine with Quadruplex DNA. *J. Am. Chem. Soc.* **1998**, *120*, 3261−3262. (b) Han, F. X.; Wheelhouse, R. T.; Hurley, L. H. Interactions of TMPyP4 and TMPyP2 with Quadruplex DNA. Structural Basis for the Differential Effects on Telomerase Inhibition. *J. Am. Chem. Soc.* **1999**, *121*, 3561−3570.

(16) Federoff, O. V.; Salazar, M.; Han, H.; Chemeris, V. V.; Kerwin, S. M.; Hurley, L. H. NMR−Based Model of a Telomerase-Inhibiting Compound Bound to G-Quadruplex DNA. *Biochemistry* **1998**, *37*, 12367−12374.

(17) Wang, Y.; Patel, D. J. Solution Structure of the Human Telomeric Repeat $d[AG_3(T_2AG_3)_3]$ G-Tetraplex. *Structure* **1993**, *1*, 263−282.

(18) Perry, P. J.; Read, M. A.; Davies, R. T.; Gowan, S. M.; Reszka, A. P.; Wood, A. A.; Kelland, L. R.; Neidle, S. 2,7-Disubstituted Amidofluorenone Derivatives as Inhibitors of Human Telomerase. *J. Med. Chem.* **1999**, *42*, 2679−2684.

(19) Harrison, R. J.; Gowan, S. M.; Kelland, L. R.; Neidle, S. Human Telomerase Inhibition by Substituted Acridine Derivatives. *Bioorg. Med. Chem. Lett.*, in press.

(20) Åqvist, J.; Medina, C.; Samuuelsson, J.-E. A New Method for Predicting Binding Affinities in Computer-aided Drug Design. *Protein Eng.* **1994**, *7*, 385−391.

(21) Luty, B. A.; Wasserman, Z. R.; Stouten, P. F. W.; Hodge, C. N.; Zacharias, M.; McCammon, J. A. A Molecular Mechanics/Grid Method for Evaluation of Ligand−Receptor Interactions. *J. Comput. Chem.* **1995**, *16*, 454−464.

(22) Eliel, E. L.; Wilen, S. H. *Stereochemistry of Organic Compounds*. John Wiley: New York, 1994, pp 765−767.

(23) Han, H.; Hurley, L. H.; Salazar, M. A DNA Polymerase Stop Assay for G-Quadruplex-Interactive Compounds. *Nucleic Acids Res.* **1999**, *27*, 537−542.

(24) INSIGHTII Modelling Environment. Molecular Simulations Inc.: San Diego, 1999.

(25) Phillips, K.; Dauter, Z.; Murchie, A. I. H.; Lilley, D. M. J.; Luisi, B. The Crystal Structure of a Parallel-stranded Guanine Tetraplex at 0.95 Angstrom Resolution. *J. Mol. Biol.* **1997**, *273*, 171−182.

JM990287E